ARTICLES
PUBLISHED ONLINE: 15 MAY 2017 | DOI: 10.1038/NGEO2952
nature geoscience

Deep and shallow long-period volcanic seismicity linked by fluid-pressure transfer

N. M. Shapiro[1,2*], D. V. Droznin[3], S. Ya. Droznina[3], S. L. Senyukov[3], A. A. Gusev[2,3] and E. I. Gordeev[2,3]

Volcanic long-period earthquakes are attributed to pressure fluctuations that result from unsteady mass transport in the plumbing system of volcanoes. Whereas most of the long-period seismicity is located close to the surface, the volcanic deep long-period earthquakes that occur in the lower crust and uppermost mantle reflect the activity in the deep parts of magmatic systems. Here, we present observations of long-period earthquakes that occurred in 2011–2012 within the Klyuchevskoy volcano group in Kamchatka, Russia. We show two distinct groups of long-period sources: events that occurred just below the active volcanoes, and deep long-period events at depths of ∼30 km in the vicinity of a deep magmatic reservoir. We report systematic increases of the long-period seismicity levels prior to volcanic eruptions with the initial activation of the deep long-period sources that reflects pressurization of the deep reservoir and consequent transfer of the activity towards the surface. The relatively fast migration of the long-period activity suggests that a hydraulic connection is maintained between deep and shallow magmatic reservoirs. The reported observations provide evidence for the pre-eruptive reload of the shallow magmatic reservoirs from depth, and suggest that the deep long-period earthquakes could be used as a reliable early precursor of eruptions.

Magmatic and hydrothermal volcanic systems generate earthquakes and tremors with periods that are longer than those for typical tectonic earthquakes of similar sizes[1–6]. The mechanisms involved in the generation of this long-period (LP) seismicity are also believed to be different from those of tectonic earthquakes[3]. It is most often interpreted as reflecting pressure fluctuations within magmatic and hydrothermal fluids, and is considered as a reliable precursor of volcanic eruptions[2–4]. Most reported volcanic LP seismicity has been observed close to the surface and reflects the activity within shallow magmatic reservoirs and hydrothermal systems. In this context, volcanic deep long-period (DLP) earthquakes[7–10] that occur in the lower crust and the uppermost mantle are particularly interesting, because they can reflect the pressurization of deep-seated parts of the magmatic systems and the magma and pressure transfer towards the surface. Alternatively, DLP generation has been attributed to the cooling of the magma diapirs that stagnate near the Moho[10]. A possible relation between the source properties of the DLP seismicity and the tectonic tremors and low-frequency earthquakes[11–13] has also been suggested[8]. For the latter the fluid pressure is one of the main controlling parameters[11,14,15]. Changes in fluid pressure may also be involved in seismic triggering of the volcanic unrest[16]. One of the main difficulties in studies of DLP events is that their numbers reported to date are small, from a few to a few hundred reported for individual volcanoes, which is marginal compared to the huge catalogues of tectonic and shallow volcanic LP seismicity.

Klyuchevskoy volcano group

Here, we present observations of the abundant deep and shallow LP seismicity within the Klyuchevskoy volcano group (KVG) in Kamchatka, Russia. The KVG is one of the largest and most active clusters of subduction-zone volcanoes in the world, and is composed of 13 closely located stratovolcanoes (Fig. 1). The 4,750-m-high Klyuchevskoy volcano is the most prominent of this cluster, and has had a mean eruptive rate of $1\,m^3\,s^{-1}$ over the past 10 kyr (ref. 17). Bezymianny and Tolbachik volcanoes have also produced strong eruptions over recent decades[17–23]. The KVG is located in a unique tectonic setting (Fig. 1), above the edge of the Pacific plate at the Kamchatka–Aleutian junction where the Hawaii–Emperor Seamount chain is subducted. Geodynamic models that have been proposed to explain the exceptional activity of the KVG include fluid being released from the thick, highly hydrated Hawaii–Emperor Seamount crust[24], mantle flow around the corner of the Pacific plate[25], and recent detachment of a portion of the subducting slab[26].

Detection of long-period volcano earthquakes

The KVG is monitored by a seismic network that is operated by the Kamchatka Branch of the Geophysical Survey of the Russian Academy of Sciences[18,22]. The positions of the 12 stations used in the present study are shown in Fig. 1. The abundant seismic activity of the KVG volcanoes includes long periods of sustained tremors[22] and numerous volcano tectonic[18–20] and LP[18,21,27,28] events. The latter mostly occur at two depth ranges[18]: above 5 km and close to 30 km. The magnitudes (see Methods) of shallow and deep LP events are comparable and most of the time do not exceed 2.5, with the strongest shallow event reaching $M = 3.1$ during days preceding volcanic eruptions[18]. An example is shown in Fig. 2a, which illustrates two hours of continuous records (that is, the N component) from station KMN on 26 June 2012. A close inspection of this record reveals that most of its weak signals are LP events (Supplementary Fig. 1). Moreover, the waveforms of many of these events are very similar to each other, which suggests that they are generated by repetitive sources. To classify these events into multiplet families, we analysed the continuous records from 2012, and identified templates that had great similarity across all of these events (see Methods). These templates (Supplementary Fig. 1) were used for initial matched-filter detection of the repeated events, based on the vertical-component records of the single stations. The waveforms for all of these recorded channels were stacked using their initial detection times, to form the final templates (Supplementary Fig. 2)

[1]Institut de Physique du Globe de Paris, Sorbonne Paris Cité, CNRS (UMR7154), 1 rue Jussieu, 75238 Paris, cedex 5, France. [2]Institute of Volcanology and Seismology FEB RAS, 9 Piip Boulevard, Petropavlovsk-Kamchatsky, Kamchatsky Region 683006, Russia. [3]Kamchatka Branch of the Geophysical Survey, Russian Academy of Sciences, 9 Piip Boulevard, Petropavlovsk-Kamchatsky, Kamchatsky Region 683006, Russia. *e-mail: nshapiro@ipgp.fr

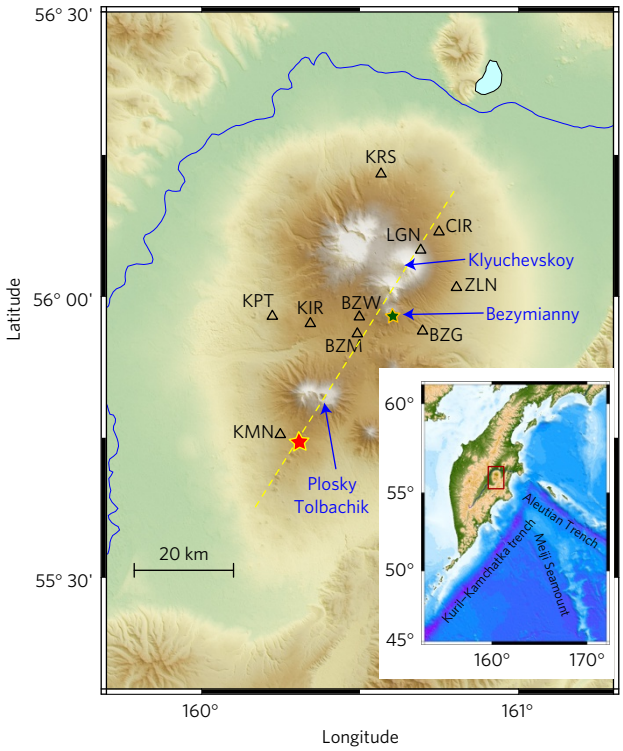

Figure 1 | Map of the Klyuchevskoy volcano group. The inset shows the general geographical and tectonic settings. Triangles show the positions of the seismic stations. The recently active volcanoes are indicated with blue arrows. The green star shows the location of three Bezymianny eruptions that occurred in 2011–2012. The red star shows the eruptive centre of the 2012–2013 Tolbachik eruption. The yellow dashed line indicates the location of the profile shown in Fig. 3a.

that were used to pick the arrival times of P-waves and S-waves and to locate the positions of the multiplet family sources (Supplementary Fig. 3). We finally proceeded with the matched-filter detection based on these multi-component templates (Fig. 2b–d).

Overall, we used 12 templates that were regrouped into four source regions (Supplementary Table 1 and Fig. 3a). The DLP source region was located at ~30 km in depth, above the assumed subcrustal magma reservoir[28], and the remaining sources are located near the surface, below the active volcanoes. The DLP events below Klyuchevskoy volcano have been systematically reported since initiation of the regular seismological monitoring of the KVG[27], and it has been suggested that they are related to the eruptions of Klyuchevskoy volcano[19].

A network-based matched-filter approach (see Methods) resulted in a large number of robust detections (Supplementary Table 1) that we used here to follow the evolution of the different LP sources with time. These detections were regrouped into catalogues that correspond to four source regions (Fig. 3a), and are shown in Fig. 3b,c. We have considered here the years 2011 and 2012, which preceded the Tolbachik eruption that started on 27 November 2011[21,23], with VEI = 4. This volcano had remained quiet since 1976, and its reactivation in 2012 resulted in the largest KVG eruption of the past two decades. During the period considered, Klyuchevskoy volcano did not undergo any eruption, while Bezymianny volcano had three short explosive eruptions, on 13 April 2011, 8 March 2012, and 1 September 2012.

Long-period seismicity and eruptions

We observed clear correlation between the shallow LP activity and the eruptions of the corresponding volcanoes (Fig. 3c). The Bezymianny volcano LP sources were systematically activated more than one month prior to its three eruptions. The activity for the Tolbachik volcano LP source region showed remarkable progressive activation that started seven months before the November 2012 eruption.

The DLP source activity increased on average from the beginning of 2011, and reached its maximum level in June–July 2012 (Fig. 3b). This increase in activity was not steady, as it showed numerous bursts that lasted a few days at a time. We also clearly distinguished three episodes when the DLP activity remained elevated for more than a month: in April 2011, November 2011 to February 2012, and April to October 2012. The first of these episodes coincided approximately with the 2011 Bezymianny volcano eruptions, while the second and third episodes preceded two other Bezymianny volcano eruptions. The beginning of the last, and the strongest, of the surges of the DLP activity coincided approximately with pronounced activation of the Tolbachik volcano LP source region (Fig. 3c). Meanwhile, the average level of DLP activity started to diminish approximately five months before the Tolbachik eruption.

The activities of the shallow LP sources were interrelated. The last Bezimianny volcano eruption was followed by approximately ten days of LP quiescence below Tolbachik volcano (Supplementary Fig. 4), after which this activity started to grow more rapidly, while the Klychevskoy volcano LP source was activated at the same time. The LP event rates below Tolbachik and Klychevskoy volcanoes increased simultaneously, until October 2012, and then another change occurred in the system (simultaneous with the strong decrease in DLP events), when the Tolbachik volcano LP activity intensified even more, while the Klyuchevskoy volcano activity started to diminish.

Long-period seismicity and fluid-pressure transfer

The similarity of the waveforms from many thousands of individual LP events (including the DLP events) suggested that they were generated by repetitive excitation of stationary sources in a non-destructive process. In a volcanic environment, such sources are most likely related to sudden pressure fluctuations within the plumbing system[2,3]. Consequently, the surges in LP activity appear to be related to elevated flux and pressurization of the fluids within the conduit system.

We interpret the observed time evolution of the long-lived LP sources as reflecting the activity of the KVG plumbing system over the two years preceding the 2012 Tolbachik volcano eruption. The KVG magma is supplied from the subcrustal magma source[28] and rises into shallow reservoirs below the main active volcanoes through the complex plumbing system[17], whose structure is only partially constrained with seismic tomography[29,30] (Fig. 3a). From the beginning of 2011, on average, the activity in the deep reservoir has been growing. The first two surges of this deep LP activity were accompanied by activation of the shallow reservoir beneath Bezymianny volcano, and the cumulated pressure is likely to have been partially released during the eruptions of Bezymianny volcano in April 2011 and March 2012. The last and strongest activation of the subcrustal reservoir started in April 2012, and this was then transferred to the shallow reservoir beneath Tolbachik volcano. When the activity in the deep part reached its maximum level in June–July 2012, the Bezimianny volcano shallow reservoir was activated again, leading to an eruption on 1 September 2012, approximately two months after the maximum DLP rate was reached. This partially released the pressure within the shallow part of the conduit (as seen by the 10-day quiescent period). This event modified the plumbing system, which resulted in simultaneous acceleration of the activity beneath Tolbachik and Klyuchevskoy volcanoes. At this point, the activity within the deep part of the plumbing system started to decrease. In October 2012, the activity was channelled towards Tolbachik volcano, which resulted in its eruption on 27 November 2012.

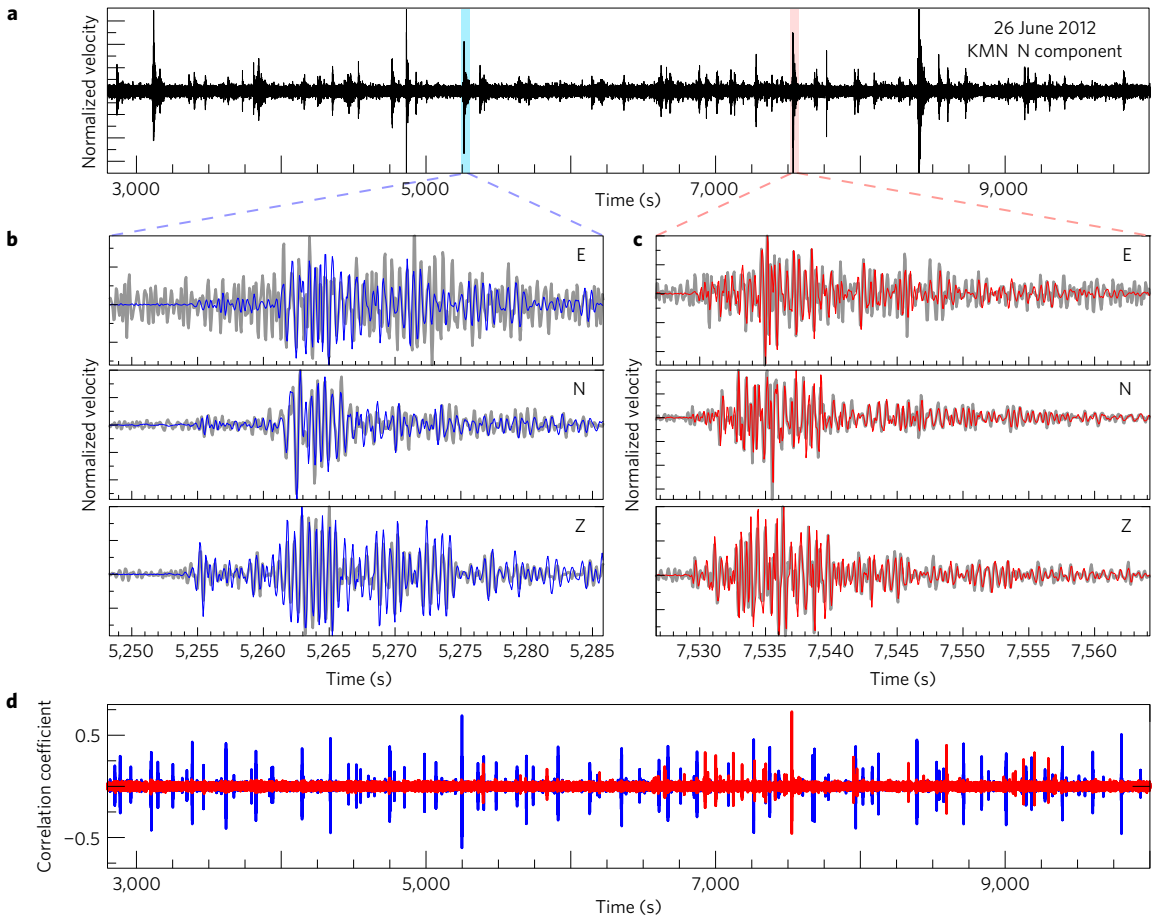

Figure 2 | Detection of repeating long-period events. a, Two hours of records (N component, station KMN, 26 June 2012) bandpass-filtered between 1 and 5 Hz. **b**, Matched-filter detection with template 1 (DLP source region; Supplementary Table 1). The scanned records and the template waveforms are shown with grey and blue lines, respectively. **c**, Similar to **b**, but for template 6 (Tolbachik LP region) shown with red lines. **d**, Results of the application of the matched filter based on templates 1 (blue line) and 6 (red line). Average correlation coefficients were computed from three-component records (see Methods) at ten and six stations for templates 1 and 6, respectively.

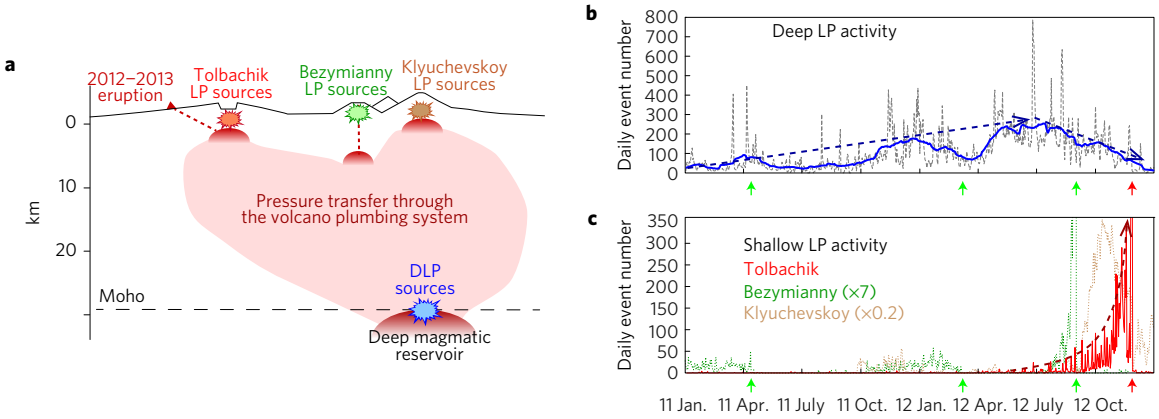

Figure 3 | Activity of the repeating long-period events. a, Cross-section along the profile indicated in Fig. 1, showing the schematic configuration of the KVG plumbing system, including three shallow reservoirs[17] and the deep reservoir[28], and the schematic locations of four groups of LP sources. **b**, Evolution of the DLP activity. Daily event numbers are shown with the grey dashed line. The solid blue line shows the activity, averaged through a sliding 41-day-long window. **c**, Daily numbers of LP events generated by shallow LP sources. The onsets of the Bezymianny and Tolbachik eruptions are indicated in **b** and **c** with the green and red arrows, respectively.

Assuming that the fluid-pressure propagation below volcanoes is governed by the diffusion equation (see Methods), we use the delay between the observed maximum of the last surge of the DLP activity and the onset of the Tolbachick eruption (five months) to approximately estimate the average hydraulic diffusivity of the feeding system as $\sim 10^2$ m^2 s^{-1}. This diffusivity, in turn, is related to the permeability of the media and to the properties of the transported fluid[31,32]. The pressure can be transmitted both by magmas and by the volatile fluids. The latter can be abundant in the shallow hydrothermal system. However, at depths of 30 km, where the DLP activity is observed, most of volatiles remain dissolved in the magma[33,34]. Therefore, we use physical properties of the andesitic

basalts[35] (average composition of the KVG magmas) to estimate the transport properties of the KVG feeding system between the deep and the shallow magmatic reservoirs. By applying the equivalent channel model for the permeability of the media[36,37], we estimate the average size of pores as being of the order of a few centimetres (see Methods), which is consistent with possible dimensions of channels filled with the liquid magma in partially molten zones below volcanoes. This result shows that the observed migration of the LP activity probably reflects the pre-eruptive transfer of the fluid pressure from the deep-seated parts of the magmatic system towards shallow magmatic reservoirs through a system of vertically connected channels, and supports the open hydraulic connection models of the dynamics of volcano-magmatic systems[38,39]. Our findings also confirm that the DLP seismicity is related to deep volcanic fluid transport[7], and can be used as reliable evidence of activation of deep parts of magmatic systems prior to major eruptions.

Methods

Methods, including statements of data availability and any associated accession codes and references, are available in the online version of this paper.

Received 2 February 2017; accepted 18 April 2017; published online 15 May 2017

References

1. Fehler, M. Observations of volcanic tremor at Mount St. Helens volcano. *J. Geophys. Res.* **88,** 3476–3484 (1983).
2. Chouet, B. A. Resonance of a fluid-driven crack: radiation properties and implications for the source of long-period events and harmonic tremor. *J. Geophys. Res.* **93,** 4375–4400 (1988).
3. Chouet, B. A. Long-period volcano seismicity: its source and use in eruption forecasting. *Nature* **380,** 309–316 (1996).
4. Chouet, B. A. & Matoza, R. S. A multi-decadal view of seismic methods for detecting precursors of magma movement and eruption. *J. Volcanol. Geotherm. Res.* **252,** 108–175 (2013).
5. Neuberg, J. W. *et al*. The trigger mechanism of low-frequency earthquakes on Montserrat. *J. Volcanol. Geotherm. Res.* **153,** 37–50 (2006).
6. Bean, C. J. *et al*. Long-period seismicity in the shallow volcanic edifice formed from slow-rupture earthquakes. *Nat. Geosci.* **7,** 71–75 (2014).
7. White, R. A. in *Fire and Mud: Eruptions and Lahars of Mount Pinatubo, Philippines* (eds Newhall, C. G. & Punongbayan, R. S.) 307–326 (Univ. Washington Press, 1996).
8. Nichols, M. L., Malone, S. D., Moran, S. C., Thelen, W. A. & Vidale, J. E. Deep long-period earthquakes beneath Washington and Oregon volcanoes. *J. Volcanol. Geotherm. Res.* **200,** 116–128 (2011).
9. Aso, N., Ohta, K. & Ide, S. Tectonic, volcanic, and semi-volcanic deep low-frequency earthquakes in western Japan. *Tectonophysics* **600,** 27–40 (2013).
10. Aso, N. & Tsai, V. C. Cooling magma model for deep volcanic long-period earthquakes. *J. Geophys. Res.* **119,** 8442–8456 (2014).
11. Obara, K. Nonvolcanic deep tremor associated with subduction in southwest Japan. *Science* **296,** 1679–1681 (2002).
12. Nadeau, R. M. & Dolenc, D. Nonvolcanic tremors deep beneath the San Andreas Fault. *Science* **307,** 389 (2005).
13. Shelly, D. R., Beroza, G. C., Ide, S. & Nakamula, S. Low-frequency earthquakes in Shikoku, Japan, and their relationship to episodic tremor and slip. *Nature* **442,** 188–191 (2006).
14. Kao, H. *et al*. A wide depth distribution of seismic tremors along the northern Cascadia margin. *Nature* **436,** 841–844 (2005).
15. Frank, W. B. *et al*. Along-fault pore-pressure evolution during a slow-slip event in Guerrero, Mexico. *Earth Planet. Sci. Lett.* **413,** 135–143 (2015).
16. Manga, M. & Brodsky, E. Seismic triggering of eruptions in the far field: volcanoes and geysers. *Annu. Rev. Earth Planet. Sci.* **34,** 263–291 (2006).
17. Fedotov, S. A., Jarinov, N. A. & Gontovaya, L. I. The magmatic system of the Klyuchevskaya group of volcanoes inferred from data on its eruptions, earthquakes, deformation, and deep structure. *J. Volcanol. Seismol.* **4,** 1–33 (2010).
18. Senyukov, S. L. *Forecasting of the Eruptions of Volcanoes Klyuchevskoy and Bezymianny at Kamchatka* [in Russian] (Lambert Academic, 2013).
19. Senyukov, S. L., Droznina, S. Ya., Nuzhdina, I. N., Garbuzova, V. T. & Kozhevnikova, T. Y. Studies in the activity of Klyuchevskoi volcano by remote sensing techniques between January 1, 2001, and July 31, 2005. *J. Volcanol. Seismol.* **3,** 50–59 (2009).
20. Thelen, W., West, M. & Senyukov, S. Seismic characterization of the fall 2007 eruptive sequence at Bezymianny volcano, Russia. *J. Volcanol. Geotherm. Res.* **194,** 201–213 (2010).
21. Senyukov, S. L. *et al*. Seismic monitoring of the Plosky Tolbachik eruption in 2012–2013 (Kamchatka Peninsula Russia). *J. Volcanol. Geotherm. Res.* **307,** 47–59 (2015).
22. Droznin, D. V. *et al*. Detecting and locating volcanic tremors on the Klyuchevskoy group of volcanoes (Kamchatka) based on correlations of continuous seismic records. *Geophys. J. Int.* **203,** 1001–1010 (2015).
23. Kugaenko, Y., Titkov, N. & Saltykov, V. Constraints on unrest in the Tolbachik volcanic zone in Kamchatka prior to the 2012–13 flank fissure eruption of Plosky Tolbachik volcano, from local seismicity and GPS data. *J. Volcanol. Geotherm. Res.* **307,** 38–46 (2015).
24. Dorendorf, F., Wiechert, U. & Wörner, G. Hydrated sub-arc mantle: a source for the Kluchevskoy volcano, Kamchatka/Russia. *Earth Planet. Sci. Lett.* **175,** 69–86 (2000).
25. Yogodzinski, G. M. *et al*. Geochemical evidence for the melting of subducting oceanic lithosphere at plate edges. *Nature* **409,** 500–504 (2001).
26. Levin, V., Shapiro, N. M., Park, J. & Ritzwoller, M. H. Seismic evidence for catastrophic slab loss beneath Kamchatka. *Nature* **418,** 763–767 (2002).
27. Gorelchik, V. I., Garbuzova, V. T. & Storcheus, A. V. Deep-seated volcanic processes beneath Klyuchevskoi volcano as inferred from seismological data. *J. Volcanol. Seismol.* **6,** 21–34 (2004).
28. Levin, V., Droznina, S., Gavrilenko, M., Carr, M. & Senyukov, S. Seismically active sub-crustal magma source of the Klyuchevskoy volcano in Kamchatka, Russia. *Geology* **42,** 983–986 (2014).
29. Koulakov, I. *et al*. Feeding volcanoes of the Kluchevskoy group from the results of local earthquake tomography. *Geophys. Res. Lett.* **38,** L09305 (2011).
30. Ivanov, A. I. *et al*. Magma source beneath the Bezymianny volcano and its interconnection with Klyuchevskoy inferred from local earthquake seismic tomography. *J. Volcanol. Geotherm. Res.* **323,** 62–71 (2016).
31. Barenblatt, G. I., Zheltov, I. P. & Kochina, I. N. Basic concepts in the theory of seepage of homogeneous liquids in fissured rocks. *J. Appl. Math. Mech.* **24,** 1286–1303 (1960).
32. Yang, D., Li, Q. & Zhang, L. Propagation of pore pressure diffusion waves in saturated porous media. *J. Appl. Phys.* **117,** 134902 (2015).
33. Carroll, M. R. & Holloway, J. R. (eds) *Volatiles in Magma* Vol. 30 (Reviews in Mineralogy, Minerological Society of America, 1994).
34. Wallace, P. & Anderson, T. A. Jr in *Encyclopedia of Volcanoes* (ed. Sigurdsson, H.) 149–170 (Academic, 2000).
35. Spera, F. J. in *Encyclopedia of Volcanoes* (ed. Sigurdsson, H.) 171–190 (Academic, 2000).
36. Paterson, M. S. The equivalent channel model for permeability and resistivity in fluid-saturated rock—a re-appraisal. *Mech. Mater.* **2,** 345–352 (1983).
37. Costa, A. Permeability-porosity relationship: a reexamination of the Kozeny–Carman equation based on a fractal pore-space geometry assumption. *Geophys. Res. Lett.* **33,** L02318 (2006).
38. Mériaux, C. & Jaupart, C. Simple fluid dynamic models of volcanic rift zones. *Earth Planet. Sci. Lett.* **136,** 223–240 (1995).
39. Pinel, V., Jaupart, C. & Albino, F. On the relationship between cycles of eruptive activity and growth of a volcanic edifice. *J. Volcanol. Geotherm. Res.* **194,** 150–164 (2010).

Acknowledgements

We thank members of the Kamchatka Branch of the Geophysical Survey of the Russian Academy of Sciences who contributed to the operation of the seismic network and to collecting and archiving the data, and C. Jaupart, E. Kaminski, W. Frank and M. Campillo for helpful discussions. This study was supported by the Russian Science Foundation (grant 14-47-00002), by the French projects 'Labex UnivEarth' and Universiteé Sorbonne Paris Cité project 'VolcanoDynamics' and by the Russian Academy of Science (research contract AAAA-A16-116070550058-4). Computations were performed using the infrastructure of the Institute of Volcanology and Seismology and of the Kamchatka Branch of the Geophysical Survey, as well of the IPGP High-Performance Computing infrastructure S-CAPADE (supported by the Île-de-France region via the SEASAME programme, by France-Grille, and by the CNRS MASTODONS programme).

Author contributions

N.M.S. and D.V.D. analysed the continuous seismograms and the repeater catalogues. S.Y.D. and S.L.S. carried out the template source location. All of the authors contributed to interpretation of the data, discussions of the results and preparation of the manuscript.

Additional information

Supplementary information is available in the online version of the paper. Reprints and permissions information is available online at www.nature.com/reprints. Publisher's note: Springer Nature remains neutral with regard to jurisdictional claims in published maps and institutional affiliations. Correspondence and requests for materials should be addressed to N.M.S.

Competing financial interests

The authors declare no competing financial interests.

Methods

The main goal of this data analysis was to detect repeatable long-period (LP) events generated by different sources. For this detection, we first identified potential templates, to form multiplet families based on analysis of waveform similarities of the detected impulsive events. To limit the amount of computation, the initial template search was based on analysis of single-component records. As we were mainly interested in the LP activity that preceded the 2012 Tolbachik volcano eruption, the initial template search used vertical-component records from the stations located near to this volcano (that is, KIR, BZW, BZG, KMN), in 2012.

Identification of potential one-component templates from the daily records. We started with an analysis of the daily vertical-component records from the individual stations, which were bandpass-filtered between 1 Hz and 5 Hz, as a typical frequency range for LP signals. We computed signal envelopes and smoothed these within a 10-s sliding window. We used the smoothed envelopes to detect all of the maxima with signal-to-noise ratios above two. Then, we retained 37.5-s-long waveforms that were centred at the positions of the detected maxima, as the impulsive signals. We computed the normalized cross-correlation functions between all of the pairs of detected impulsive signals, and used their maxima for estimations of the correlation coefficients (CCs). The matrix of these CCs was used to regroup the detected impulsive signals into families of similar events. At this step, we considered CCs below 0.44 as not significant, and the corresponding elements of the CC matrix were set to zero. For every impulsive signal, we computed the sum of its CCs (CCsum) with all of the other events (the sum of the non-diagonal elements of the corresponding raw data of the CC matrix). We then selected the signal with the largest CCsum as the master event, and grouped into a multiplet family all of the other signals with CCs between them and the master event of above 0.44. This procedure was iteratively repeated for the remaining impulsive signals, to identify all of the possible multiplet families. We then retained the master events from the multiplets with more than five members for use in the following steps of the analysis.

Identification of potential one-component templates in 2012. The procedure described above was applied to the vertical-component records from every day in 2012. The ensemble of selected master events was classified, in turn, into multiplet families based on their CCs, with the same criteria as described in the previous section. Similarly, the master events from multiplets with more than five members were retained for use in the following steps of the analysis.

Matched-filter detection based on the one-component templates. The selected master events were used as templates for the matched-filter detection. This detection was based on computing the CCs between the template waveforms and the scanned continuous records in a sliding window of the same length as the template (37.5 s). We considered CCs above 0.44 as the detection threshold. Also, we considered that the approach used could not resolve detections in time that were separated by less the one quarter of the template length (that is, 9.375 s). Therefore, when such closely located detections were found, we retained only those with the highest CCs. We then rejected the templates that resulted in less than 250 detections and those that mostly produced detections dominated by instrumental noise. The remaining catalogues were compared, to group together those with redundant sets of detections[40]. After this processing, we retained the 12 templates listed in Supplementary Table 1, with their typical waveforms and spectra illustrated in Supplementary Fig. 1.

Multi-component templates. For the retained templates, we stacked all of the waveforms that corresponded to detections with CCs above 0.65. This stacking was performed not only at the station and the component where the template was initially identified, but also at all of the stations and all of the three components. As a result, multi-station templates were constructed (Supplementary Fig. 2). These stacked waveforms with high signal-to-noise ratios were used to measure the travel times of P-waves and S-waves, and to locate the hypocentres of the template sources (Supplementary Fig. 3). These hypocentres formed four groups (Fig. 3a). Then, the multi-station templates were used to perform the final LP event detections for 2011 and 2012, according to the network-based matched-filter approach[41]. For the DLP events and the events below Klyuchevskoy and Bezymianny volcanoes, we used ten stations (30 components): KRS, CIR, LGN, ZLN, KPT, KIR, BZW, BZM, BZG and KMN. For the events below Tolbachik volcano, we used only the six stations (18 components) that were relatively close to this volcano: KPT, KIR, BZW, BZM, BZG and KMN. As the detection threshold, we set the value of the average multi-station correlation coefficient above 0.12, which was approximately sevenfold greater than the root mean square level during the periods without LP activity. Finally, we combined the detections for the templates from the same source group. Again, we considered that the matched-filter method used cannot resolve detections separated by less than one quarter of the template length in time (9.375 s). Therefore, when such closely located detections were found, we retained only those with the highest CCs.

Fluid-pressure pulse propagation through porous rocks. Evolution of pressure P of a fluid filtrating through a homogeneous porous medium is governed by a diffusion equation[31,32]:

$$\frac{dP}{dt} = D\frac{\partial^2 P}{\partial x^2}$$

where t is time, x is distance, and D is hydraulic diffusivity. We approximate the problem of propagation of pressure pulse in the following way. At time $t=0$ the pressure perturbation of size P_0 is created at depths $x<0$, while $P=0$ for $x>0$. We then solve the diffusion equation for $x>0$ with the above described initial condition and the boundary condition $P(x=0)=P_0$. The solution is obtained as:

$$P(x,t) = P_0\left(1-\mathrm{erf}\left(\frac{x}{\sqrt{4Dt}}\right)\right)$$

where erf is the error function. At a given location, the pressure approximately reaches the level of $P_0/2$ when the argument of the error function becomes 0.5. The characteristic time of propagation of pressure pulse over distance l becomes:

$$t_l = \frac{l^2}{D}$$

We estimate the time t_l as approximately equal to five months from the delay between the observed maximum of the last surge of the DLP activity and the onset of the Tolbachick eruption. l is estimated from the distance between the DLP and the Tolbachick LP sources as 40 km, resulting in $D \approx 10^2\ \mathrm{m^2\ s^{-1}}$. The hydraulic diffusivity is related to the permeability of the media and to the properties of the transported fluid[31,32]:

$$D = \frac{kK}{\phi\eta}$$

where k and ϕ are the permeability and the porosity of the media and K and η are the bulk modulus and the viscosity of the fluid. Finally, we use the equivalent channel model[36,37] to express the media permeability in terms of the average effective size of pores. Assuming the cylindrical shape of the pores, this theory gives:

$$k = \frac{\phi}{\tau}\frac{r^2}{8} \qquad D = \frac{Kr^2}{\tau 8\eta}$$

where r is the hydraulic radius (average effective radius of pores) and τ is the average channel tortuosity, defined as the square of the ratio between the effective channel length due to the tortuous path and the length through which the fluid was transported in the media. For the andesitic basalt[35]: $K \approx 10^{10}$ Pa and $\eta \approx 10^3$ Pa. We consider that for a system of well-connected pores the tortuosity is close to 1 and obtain $r \approx 10^{-2}$ m.

Estimation of earthquake magnitudes. The Kamchatka Branch of Russian Geophysical Survey uses the modified regional magnitude scale[42,43]:

$$M = \log_{10} U + f(t_{S\text{-}P})$$

$$f(t_{S\text{-}P}) = \begin{cases} 1.42\log_{10}(t_{S\text{-}P}) + 0.72, & t_{S\text{-}P} < 7\,\mathrm{s} \\ 2.44\log_{10}(t_{S\text{-}P}) - 0.14, & t_{S\text{-}P} \geq 7\,\mathrm{s} \end{cases}$$

where U is the maximum S-wave ground velocity between 0.5 and 10 Hz in $\mu\mathrm{s}^{-1}$ and $t_{S\text{-}P}$ is the arrival time difference between S- and P-waves.

Data availability. The seismological time series used for the analysis are available from the Kamchatka Branch of the Geophysical Survey of Russian Academy of Sciences (http://www.emsd.ru) on request.

References

40. Frank, W. B. *et al*. Using systematically characterized low-frequency earthquakes as a fault probe in Guerrero, Mexico. *J. Geophys. Res.* **119,** 7686–7700 (2014).
41. Gibbons, S. J. & Ringdal, F. The detection of low magnitude seismic events using array-based waveform correlation. *Geophys. J. Int.* **165,** 149–166 (2006).
42. Fedotov, S. A. *Energy Classification of the Kuril-Kamchatka Earthquakes and the Problem of Magnitudes* [in Russian] (Nauka, 1972).
43. Gusev, A. A. & Melnikova, V. N. Correlations between world and Kamchatka magnitudes. *J. Volcanol. Seismol.* **6,** 55–63 (1990).